Electronic Supplementary Material (ESI) for Journal of Materials Chemistry A
This journal is © The Royal Society of Chemistry 2013

Electronic Supplementary Information (ESI)

Role of Transition Metal Nanoparticles in Extra Lithium Storage Capacity of Transition Metal Oxides: A Case Study of Hierarchical Core-Shell Fe_3O_4@C and Fe@C Microspheres

Liwei Su[a,b], Yiren Zhong[a] and Zhen Zhou[a,*]

[a] Tianjin Key Laboratory of Metal and Molecule Based Material Chemistry, Key Laboratory of Advanced Energy Materials Chemistry (Ministry of Education), Institute of New Energy Material Chemistry, Synergetic Innovation Center of Chemical Science and Engineering (Tianjin), Nankai University, Tianjin 300071, China.

[b] State Key Laboratory Breeding Base of Green Chemistry-Synthesis Technology, College of Chemical Engineering and Material Science, Zhejiang University of Technology, Hangzhou, Zhejiang, 310032, China

Email: zhouzhen@nankai.edu.cn

This journal is © The Royal Society of Chemistry 2013

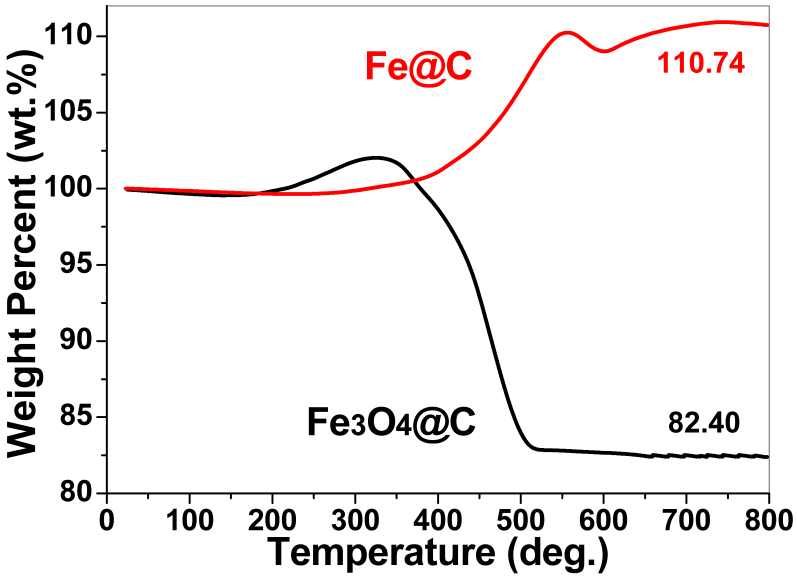

Fig. S1. Thermogravimetric analysis (TGA) of Fe_3O_4@C and Fe@C composites.

To confirm the carbon content in these composites and its corresponding contribution to lithium storage capacity, TGA was performed in air at 10 °C min^{-1} (Fig. S1). After gradually heating up to 800 °C, the final weight percents of Fe_3O_4@C and Fe@C were 82.40 and 110.74 wt.%, respectively. During the heating process, two oxidation reactions happened at the same time. One was the oxidation of Fe_3O_4 and Fe to Fe_2O_3 to increase sample weight. The other was the oxidation of carbon shell to CO_2 leading to weight loss. Thus, we can roughly calculated the carbon contents in Fe_3O_4@C and Fe@C composites to be approximate 20.3 and 22.6 wt.%, respectively.

This journal is © The Royal Society of Chemistry 2013

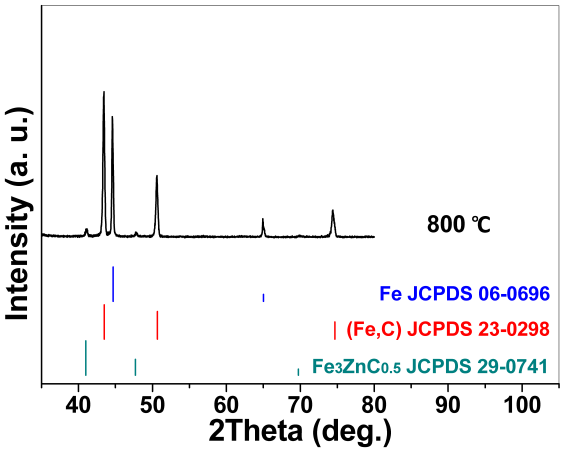

Fig. S2. XRD patterns of the final Fe@C composites.

Fig. S2 shows the XRD patterns of the heated samples at 800 °C. The peaks at 44.7° and 65.0° correspond to (110) and (200) planes of α-Fe (JCPDS 06-0696, with the body-centered-cubic structure), while the peaks at 43.5°, 50.7°, and 74.7° are well assigned to (111), (200), and (220) planes of γ-Fe ((Fe, C) solid solution phase, JCPDS 23-0298, with the face-centered-cubic structure).[1-4] Besides, very weak peaks at 41.0°, 47.7°, and 69.8° are in agreement with the standard card of cubic $Fe_3ZnC_{0.5}$ with space group of Pm-3m (JCPDS 29-0741). Note that, no other metals than Fe were introduced in the whole synthesis procedure; therefore, Fe atom should replace the position of Zn and the trace impurity should be Fe_8C.[5-8]

This journal is © The Royal Society of Chemistry 2013

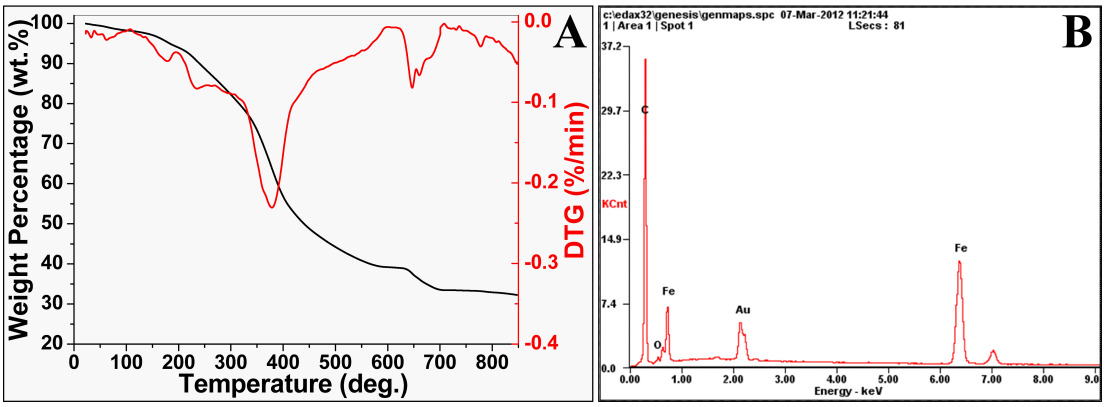

Fig. S3. TG curves of Fe_3O_4@C composites derived from the hydrothermal route before sintering at high temperatures (A). Electron diffraction spectra (EDS) of the final Fe@C composites (B).

TG measurements were performed in Ar atmosphere to confirm the phase transformation of the hydrothermal product along with the increasing temperatures (Fig. S2A). During the heating process, two dramatic drops were observed in the TG curve. The first drop before 550 °C corresponded to the loss of H_2O and the carbonization of carboneous materials decomposed from the hydrothermal glucose solution. The second drop is located at around 650-700 °C, belonging to the oxygen loss from Fe_3O_4 to FeO and Fe. The two platforms at the range of 550-650 °C and after 700 °C demonstrate the component stability of Fe_3O_4@C and Fe@C composites in the corresponding temperature range, respectively. A slight weight loss still exists in the TG curve after 800 °C. EDS was also performed to further confirm the oxygen content in the final Fe@C composites as 1.8 wt.% (Fig. S2B). Although it is difficult to remove the oxygen in Fe_3O_4@C composites completely, the existence of trace oxygen can contribute very little lithium storage based on the traditional conversion mechanism (Type III) and have no influence on the conclusion.

This journal is © The Royal Society of Chemistry 2013

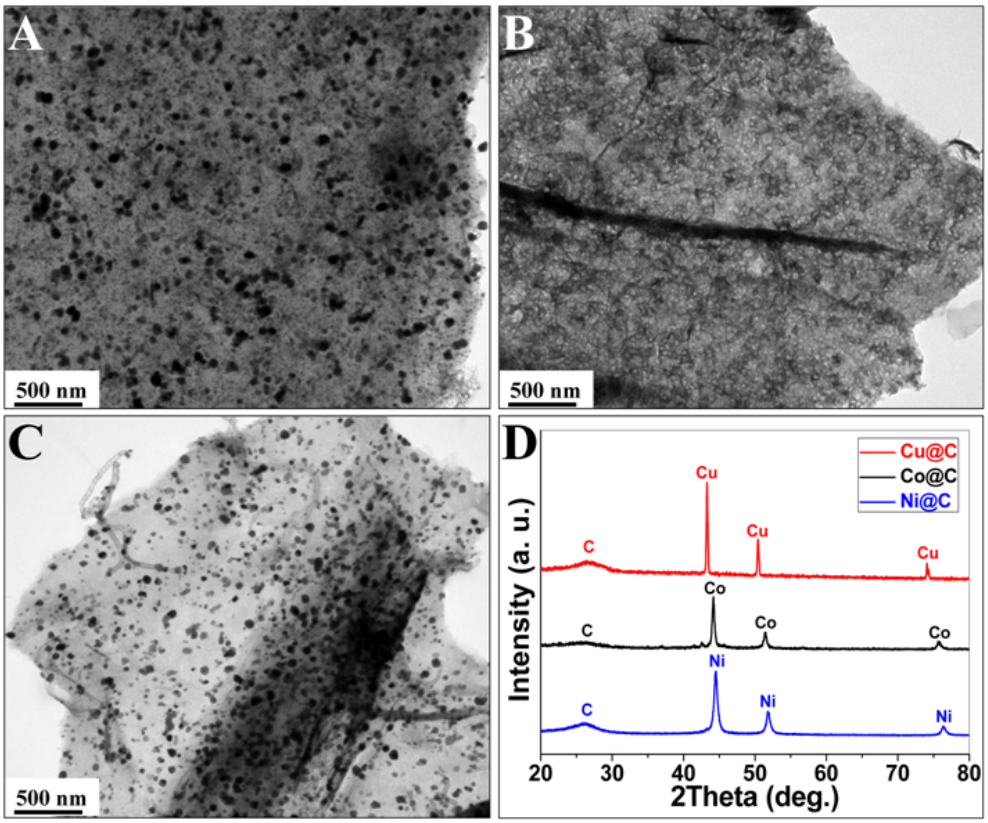

Fig. S4. TEM images of Co@C (A), Cu@C (B), Ni@C (C) composites and corresponding XRD patterns (D).

Preparation of highly-dispersed Co@C, Cu@C, and Ni@C nanosheets

In a typical synthesis, 10.00 g urea, 1.00 citric acid, and 0.8 g metal chlorides were dissolved in the mixture solution of 150 mL ethanol and 50 mL distilled water with continuous stirring at 75 °C for ~3 h until the formation of gel, then transferred into an oven to keep 100 °C over night. The as-prepared solid mixture was sintered at high temperatures of 350 °C for 4 h and 650 °C for 10 h in Ar atmosphere. The obtained black products were grinded and stored for further characterization.

This journal is © The Royal Society of Chemistry 2013

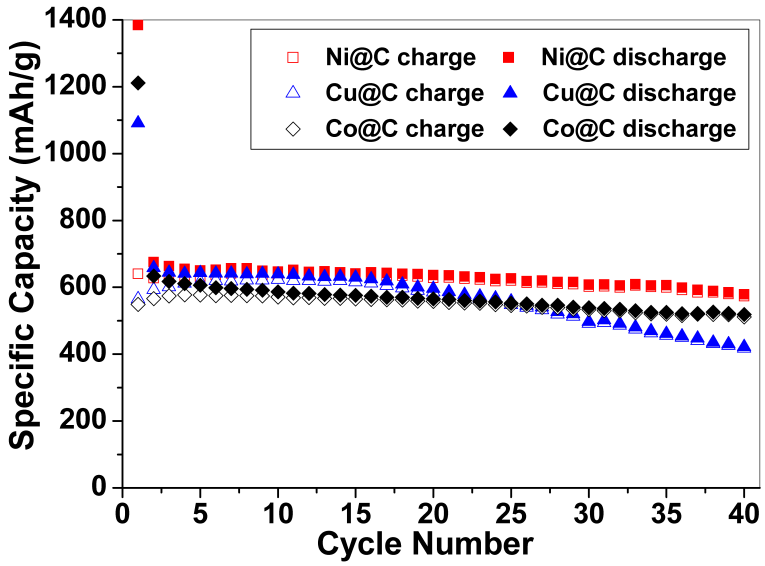

Fig. S5. Cycling performances of highly-dispersed Co@C, Cu@C and Ni@C electrodes at 200 mA g^{-1}.

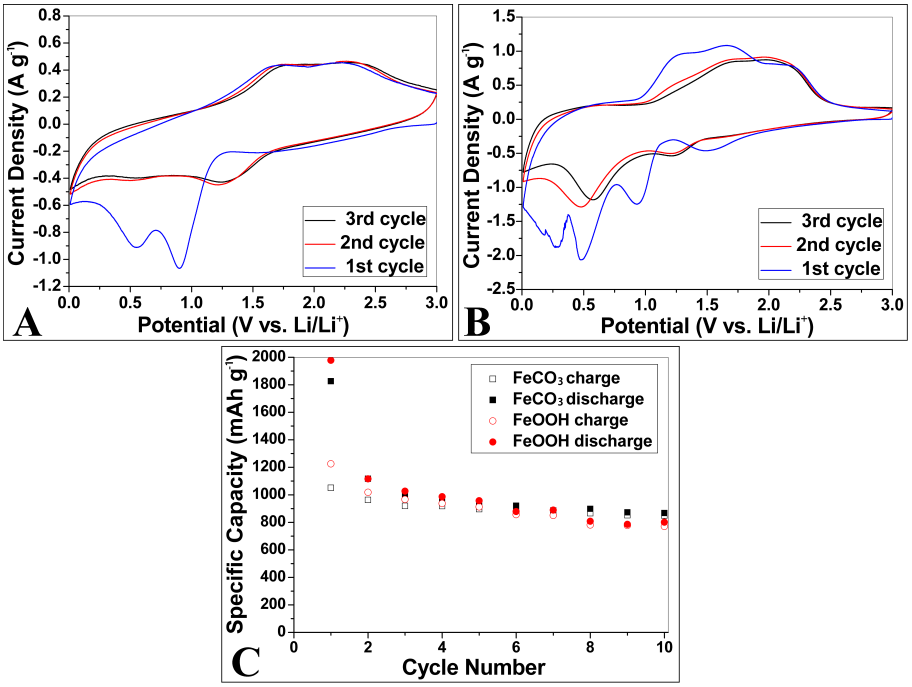

Fig. S6. CV curves of commercialized $FeCO_3$ (A) and FeOOH (B). Cycling performances of commercialized $FeCO_3$ and FeOOH electrodes at 200 mA g^{-1} (C).

This journal is © The Royal Society of Chemistry 2013

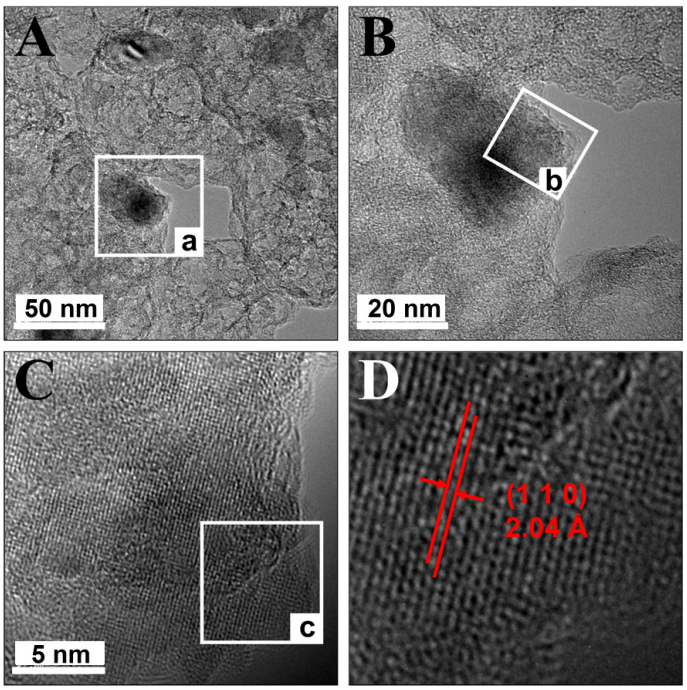

Fig. S7. HRTEM images of Fe@C electrodes after the initial charge. B, C and D correspond to the white region a, b and c, respectively.

Electronic Supplementary Material (ESI) for Journal of Materials Chemistry A
This journal is © The Royal Society of Chemistry 2013

Table S1. Extra capacity phenomenon of MOs and corresponding explanations reported in previous works.

Active materials	TC[a] of MOs (mAh g^{-1})	Tested capacity (mAh g^{-1})	Current density (mA g^{-1})	Cycling number	Explanation	Refs
Mesoporous Fe_3O_4@C nanorods	928	1010[b]	92.8	50	No explanation	9
Graphene-coated hollow Fe_3O_4	928	900	50	50	No explanation	10
Graphene/Fe_3O_4 aerogel	928	1100	200	50	No explanation	11
Graphene-encapsulated Fe_3O_4	928	950	35	85	Reversible polymeric gel-like film	12
Fe_3O_4/graphene	928	1000	2000	100	Reversible polymeric gel like film	13
Fe_3O_4 nanorods/SWCNT	928	>1000	928	50	Reversible polymeric gel-like film	14
Hollow porous Fe_3O_4 beads/RGO	928	1039	100	170	Reversible polymeric gel-like film	15
Fe_3O_4/C micro-flowers	928	1030	185	150	Reversible polymeric gel like film Possible interfacial lithium storage	16
Au-Co_3O_4 nanowires	890	>1000	34	8	Reversible polymeric gel-like film	17
Co_3O_4 porous nanocapsules	890	1000	130	20	Favorable features of unique nanostrucures	18
Co_3O_4/graphene	890	935	50	30	Active graphene surface; grain Co_3O_4 boundary	19
Co_3O_4/graphene	890	1065	445	30	Abundant nanocavities or defects of graphene; Co_3O_4 porous sheets	20
Co_3O_4 nanorods/graphene	890	1090	1000	40	No explanation	21
Needlelike Co_3O_4 nanotubes	890	918	50	30	No explanation	22
Mesoporous Co_3O_4	890	1000	100	40	No explanation	23
Foam-like Co_3O_4 nanosheets	890	900	178	10	No explanation	24
Mesoporous Co_3O_4	890	1240	100	30	No explanation	25
Co_3O_4 porous nanocages	890	1465	300	50	No explanation	26
3D heterostructured Co_3O_4/RGO	890	1108	50	50	High capacity of the porous RGO film	27
Porous Co_3O_4 nanorod arrays	890	~1000	111	20	Favorable features of unique nanostrucures	28
Graphene-coated mesoporous Co_3O_4	890	1150	111	30	Reversible SEI formation and dissolution	29
Hierarchical Co_3O_4 microspheres	890	1000	89	50	Favorable features of unique nanostrucures	30
Single-crystalline Co_3O_4 Nanobelts	890	980	100	60	Additional lithium storage in the grain boundaries	31
Highly ordered mesoporous Co_3O_4	890	1200	50	100	High surface area and porous structures	32
Co_3O_4 nanocages	890	970	50	30	Interfaces and pores of the porous material	33
Mesoporous Co_3O_4 nanoneedles	890	1079	150	50	Robust mesoporous structure	34
Hollow Co_3O_4 nanorods	890	903	240	20	Hollow, porous structure	35
Self-stacked Co_3O_4 nanosheets	890	107	178	50	Nanosandwich structure	36

This journal is © The Royal Society of Chemistry 2013

Active materials	TC of MOs ($mAh\ g^{-1}$)	Tested capacity ($mAh\ g^{-1}$)	Current density ($mA\ g^{-1}$)	Cycling number	Explanation	Refs
α-Fe_2O_3 hollow nanofibers	1005	1293	60	40	Pseudo-capacitance	37
Fe_2O_3@C nanocomposites	1005	1210	100	50	No explanation	38
Mesoporous CoO nanodisks	716	1119	200	50	No explanation	39
CoO quantum dot/grephene	716	1008	1000	50	No explanation	40
Porous carbon-modified MnO disks	756	1044	100	140	No explanation	41
NiO/graphene	718	1098	100	50	No explanation	42
3D-hierarchical NiO–graphene	780	1065	200	50	High capacity of graphene	43
NiO microshpheres	718	>800	50	7	Some unknown side reactions	44
Mesoporous carbon/NiO	718	1426[b]	1000	50	Reversible polymeric gel-like film	45
Nanostructure NiO	718	746	154	10	Reversible polymeric gel-like film	46
Microscale cog-like CuO films	674	810	300	30	Reversible polymeric gel-like film	47
CuO/graphene	674	700	70	30	High capacity of graphene	48
Carbon coated $ZnFe_2O_4$ nanoparticles	1000	1300	40	100	Reversible polymeric gel-like film	49
$CoFe_2O_4$/graphene sandwich	914	1047[b]	200	160	Synergistic effect between $CoFe_2O_4$ and graphene	50
$CoFe_2O_4$/graphene	914	950	150	50	No explanation	51

[a] TC means the theoretical capacity of MOs. [b] This value is based on MOs, *i.e.*, C_{MOs} calculated by Eqn. (1) in the manuscript, while others are based on the overall mass of the corresponding sample.

This journal is © The Royal Society of Chemistry 2013

Table S2. Components when discharge to ~0 V of different Fe-based anode materials and corresponding reduction/oxidation reactions and potential peaks in CV curves.

Fe-based anodes	Components (cycled to ~0 V)	Reduction peaks (1st discharge)		Reduction peaks after 1st cycle		Oxidation peaks		Test conditions	Refs
Fe_2O_3	$Fe^0 + Li_2O$ + SEI	1.57 V 0.93 V 0.54 V	Fe_2O_3 to $Li_xFe_2O_3$ Fe^{3+} to Fe^{2+} Fe^{2+} to Fe^0	0.65 V	Fe^{3+} to Fe^0	1.69 V 1.95 V	Fe^0 to Fe^{2+} Fe^{2+} to Fe^{3+}	0.2 mV s^{-1} 1 M $LiPF_6$ + EC/DMC/EMC (1:1:1)	52
FeO[a]	$Fe^0 + Li_2O$ + SEI	0.7 V	Fe^{2+} to Fe^0	1.0 V	Fe^{2+} to Fe^0	~1.6 V	Fe^0 to Fe^{3+}	1 M $LiPF_6$ + EC/DMC (1:1)	53
$FeCO_3$	$Fe^0 + Li_2O$ + Li_2CO_3 + SEI	0.55 V 0.85 V	Fe^{2+} to $Fe^0/Li_2O/Li_2CO_3$	1.3 V	Fe^0 to Fe^{2+} C^x to C^{4+}	1.7 V 2.3 V	Fe^0 to Fe^{2+} C^x to C^{4+}	0.5 mV s^{-1} 1 M $LiPF_6$ + EC/DMC/EMC (1:1:1)	Fig. S6A 54
FeC_2O_4	$Fe^0 + Li_2O$ + $Li_2C_2O_4$ + SEI	1.21 V 0.76 V	FeC_2O_4 to $Fe^0/Li_2C_2O_4$	1.3 V	FeC_2O_4 to Fe^0	1.3-1.9 V	Fe^0 to Fe^{3+}	0.1 mV s^{-1} 1 M $LiPF_6$ + EC/DEC (1:1)	55
FeF_3[a]	Fe^0 + LiF + SEI	3.0 V 1.8 V	FeF_3 to Li_xFeF_3 Li_xFeF_3 to Fe^0	-	-	2.8 V 3.25 V	Li_xFeF_3 to Fe^0 FeF_3 to Li_xFeF_3	20 μV s^{-1} 1 M $LiPF_6$ + EC/DMC (1:1)	56
FeOOH	$Fe^0 + Li_2O$ + LiOH + SEI	1.0 V 0.48 V 0.25 V	Fe^{3+} to $Fe^0/Li_2O/LiOH$ SEI formation	1.25 V 0.6 V	Fe^{3+} to $Fe^0/Li_2O/LiOH$	1.6-2.2 V	Fe^0 to Fe^{3+}	0.5 mV s^{-1} 1 M $LiPF_6$ + EC/DMC/EMC (1:1:1)	Fig. S6B
Fe_3O_4	$Fe^0 + Li_2O$ + SEI	0.8 V 0.55 V	Fe_3O_4 to $Li_xFe_3O_4$ Fe^{3+}/Fe^{2+} to Fe^0 SEI formation	1.45 V 0.6-0.9 V	Fe^{3+}/Fe^{2+} to Fe^0 Reduction of some SEI components	1.5-2.2 V	$Fe^0 \rightarrow Fe^{2+}/Fe^{3+}$ Oxidation of some SEI components	0.5 mV s^{-1} 1 M $LiPF_6$ + EC/DMC/EMC (1:1:1)	This work

This journal is © The Royal Society of Chemistry 2013

Fe@C	Fe^0 + SEI	1.2 V 0.3-0.8 V	Preliminary decomposition of electrolytes SEI formation	1.45 V 0.95 V 0.75 V	Fe^{3+}/Fe^{2+} to Fe^0 Reduction of some SEI components	1.6 V 1.9 V	$Fe^0 \rightarrow Fe^{2+}/Fe^{3+}$ Oxidation of some SEI components	0.5 mV s^{-1} 1 M $LiPF_6$ + EC/DMC/EMC (1:1:1)	This work

1 "-" means that no explanation was given.

This journal is © The Royal Society of Chemistry 2013

Table S3. Components when discharge to ~0 V of Fe_3O_4 anode materials and corresponding reduction/oxidation reactions and potential peaks in CV curves.

Fe-based anodes	Components (~0 V)	Reduction peaks (1st discharge)		Reduction peaks after 1st cycle		Oxidation peaks		Test conditions	Refs
Fe_2O_3/Fe	$Fe^0 + Li_2O$ + SEI	1.6 V	Fe_2O_3 to $Li_xFe_2O_3$	1.4 V	Fe_2O_3 to $Li_xFe_2O_3$	0.5 V	-	0.1 mV s^{-1} 1 M $LiPF_6$ + EC/DMC (1:1)	57
		0.8 V	Fe^{3+}/Fe^{2+} to Fe^{2+}	0.8 V	Fe^{3+}/Fe^{2+} to Fe^{2+}	1.5 V			
		0.2 V	SEI	0.2 V	SEI	2.0 V			
Fe_2O_3/Cu	$Cu^0 + Fe^0 + Li_2O$ + SEI	0.2-1.2 V	-	0.5 V	-	1.0 V	-		
		0.75 V		1.3 V		2.0 V			
		1.05 V		1.6 V					
Fe_3O_4	$Fe^0 + Li_2O$ + SEI	0.5 V	Fe^{3+}/Fe^{2+} to Fe^0 SEI	0.85 V	-	1.2-1.9 V	Fe^0 to Fe^{3+}/Fe^{2+}	0.1 mV s^{-1}	58
Ni/Fe_3O_4	$Ni^0 + Fe^0 + Li_2O$ + SEI	0.65 V	Fe^{3+}/Fe^{2+} to Fe^0 SEI	1.5 V 0.6-0.8 V	-	1.6-2.2 V	Fe^0 to Fe^{3+}/Fe^{2+}	1 M $LiPF_6$ + EC/DMC (1:1)	
C	Li_xC + SEI	0-0.8 V	C to Li_xC SEI	No peaks	-	No peaks	-	0.1 mV s^{-1}	
Ni/C	$Ni_0 + Li_xC$ + SEI	1.6 V	Preliminary decoposition of electrolytes	No peaks	-	1.2 V	Reversible oxidation of some SEI components	1 M $LiPF_6$ + EC/DMC/EMC (1:1:1)	59
		0.6 V	Formation of SEI films			1.6-2.5 V			

"-" means that no explanation was given.

This journal is © The Royal Society of Chemistry 2013

References

1. X.-C. Sun and N. Nava, *Nano Lett.*, 2002, **2**, 765-769.
2. P.-Z. Si, Z.-D. Zhang, D.-Y. Geng, C.-Y. You, X.-G. Zhao and W.-S. Zhang, *Carbon*, 2003, **41**, 247-251.
3. X. L. Dong, Z. D. Zhang, Q. F. Xiao, X. G. Zhao and Y. C. Chuang, *J. Mater. Sci.*, 1998, **33**, 1915-1919.
4. H. G. Kim, S. Z. Han, K. Euh and S. H. Lim, *Mater. Sci. Eng. A*, 2011, **530**, 652-658.
5. G. L. Weerasinghe, R. Needs and C. Pickard, *Phys. Rev. B*, 2011, **84**, 174110.
6. A. N. Timoshevskii, V. A. Timoshevskii and B. Z. Yanchitsky, *J. Phys. Condens. Mat.*, 2001, **13**, 1051-1061.
7. E. L. Peltzer, Y. Blancá, J. Desimoni and N. E. Christensen, *Hyperfine Interact.*, 2006, **161**, 197-202.
8. S. Nasu, T. Takano and F. E. Fujita, *Hyperfine Interact.*, 1986, **28**, 1071-1074.
9. S. M. Yuan, J. X. Li, L. T. Yang, L. W. Su, L. Liu and Z. Zhou, *ACS Appl. Mater. Interfaces*, 2011, **3**, 705-709.
10. D. Chen, G. Ji, Y. Ma, J. Y. Lee and J. Lu, *ACS Appl. Mater. Interfaces*, 2011, **3**, 3078-3083.
11. W. Chen, S. Li, C. Chen and L. Yan, *Adv. Mater.*, 2011, **23**, 5679-5683.
12. G. Zhou, D.-W. Wang, F. Li, L. Zhang, N. Li, Z.-S. Wu, L. Wen, G. Q. Lu and H.-M. Cheng, *Chem. Mater.*, 2010, **22**, 5306-5313.
13. S. K. Behera, *Chem. Commun.*, 2011, **47**, 10371-10373.
14. C. Ban, Z. Wu, D. T. Gillaspie, L. Chen, Y. Yan, J. L. Blackburn and A. C. Dillon, *Adv. Mater.*, 2010, **22**, E145-E149.
15. Y. Chen, B. Song, X. Tang, L. Lu and J. Xue, *J. Mater. Chem.*, 2012, **22**, 17656-17662.
16. S. Jin, H. Deng, D. Long, X. Liu, L. Zhan, X. Liang, W. Qiao and L. Ling, *J. Power Sources*, 2011, **196**, 3887-3893.
17. K. T. Nam, D. W. Kim, P. J. Yoo, C. Y. Chiang, N. Meethong, P. T. Hammond, Y. M. Chiang and A. M. Belcher, *Science*, 2006, **312**, 885-888.
18. J. Liu, H. Xia, L. Lu and D. Xue, *J. Mater. Chem.*, 2010, **20**, 1506-1511.
19. Z. S. Wu, W. C. Ren, L. Wen, L. B. Gao, J. P. Zhao, Z. P. Chen, G. M. Zhou, F. Li and H. M. Cheng, *ACS Nano*, 2010, **4**, 3187-3194.
20. S. Q. Chen and Y. Wang, *J. Mater. Chem.*, 2010, **20**, 9735-9739.
21. L. Tao, J. Zai, K. Wang, H. Zhang, M. Xu, J. Shen, Y. Su and X. Qian, *J. Power Sources*, 2012, **202**, 230-235.
22. X. W. Lou, D. Deng, J. Y. Lee, J. Feng and L. A. Archer, *Adv. Mater.*, 2008, **20**, 258-262.
23. K. M. Shaju, F. Jiao, A. Debart and P. G. Bruce, *Phys. Chem. Chem. Phys.*, 2007, **9**, 1837-1842.
24. Y. Fan, H. Shao, J. Wang, L. Liu, J. Zhang and C. Cao, *Chem. Commun.*, 2011, **47**, 3469-3471.
25. S. Xiong, J. S. Chen, X. W. Lou and H. C. Zeng, *Adv. Funct. Mater.*, 2012, **22**, 861-871.
26. L. Hu, N. Yan, Q. Chen, P. Zhang, H. Zhong, X. Zheng, Y. Li and X. Hu, *Chem. Eur. J.*, 2012, **18**, 8971-8977.
27. B. G. Choi, S. J. Chang, Y. B. Lee, J. S. Bae, H. J. Kim and Y. S. Huh, *Nanoscale*, 2012, **4**, 5924-5930.

This journal is © The Royal Society of Chemistry 2013

28. W. Mei, J. Huang, L. Zhu, Z. Ye, Y. Mai and J. Tu, *J. Mater. Chem.*, 2012, **22**, 9315-9321.
29. W. Yue, Z. Lin, S. Jiang and X. Yang, *J. Mater. Chem.*, 2012, **22**, 16318-16322.
30. B. Guo, C. S. Li and Z. Y. Yuan, *J. Phys. Chem. C*, 2010, **114**, 12805-12817.
31. H. Huang, W. Zhu, X. Tao, Y. Xia, Z. Yu, J. Fang, Y. Gan and W. Zhang, *ACS Appl. Mater. Interfaces*, 2012, **4**, 5974-5980.
32. G. X. Wang, H. Liu, J. Horvat, B. Wang, S. Z. Qiao, J. Park and H. Ahn, *Chem. Eur. J.*, 2010, **16**, 11020-11027.
33. N. Yan, L. Hu, Y. Li, Y. Wang, H. Zhong, X. Hu, X. Kong and Q. Chen, *J. Phys. Chem. C*, 2012, **116**, 7227-7235.
34. X. W. Lou, D. Deng, J. Y. Lee and L. A. Archer, *J. Mater. Chem.*, 2008, **18**, 4397-4401.
35. H.-W. Shim, Y.-H. Jin, S.-D. Seo, S.-H. Lee and D.-W. Kim, *ACS Nano*, 2011, **5**, 443-449.
36. X. Wang, H. Guan, S. Chen, H. Li, T. Zhai, D. Tang, Y. Bando and D. Golberg, *Chem. Commun.*, 2011, **47**, 12280-12282.
37. S. Chaudhari and M. Srinivasan, *J. Mater. Chem.*, 2012, **22**, 23049-23056.
38. S.-L. Chou, J.-Z. Wang, D. Wexler, K. Konstantinov, C. Zhong, H.-K. Liu and S.-X. Dou, *J. Mater. Chem.*, 2010, **20**, 2092-2098.
39. Y. Sun, X. Hu, W. Luo and Y. Huang, *J. Mater. Chem.*, 2012, **22**, 13826-13833.
40. C. Peng, B. Chen, Y. Qin, S. Yang, C. Li, Y. Zuo, S. Liu and J. Yang, *ACS Nano*, 2012, **6**, 1074-1081.
41. Y. Sun, X. Hu, W. Luo and Y. Huang, *J. Mater. Chem.*, 2012, **22**, 19190-19195.
42. Y. Huang, X.-l. Huang, J.-s. Lian, D. Xu, L.-m. Wang and X.-b. Zhang, *J. Mater. Chem.*, 2012, **22**, 2844-2847.
43. L. Tao, J. Zai, K. Wang, Y. Wan, H. Zhang, C. Yu, Y. Xiao and X. Qian, *RSC Adv.*, 2012, **2**, 3410-3415.
44. L. Liu, Y. Li, S. M. Yuan, M. Ge, M. M. Ren, C. S. Sun and Z. Zhou, *J. Phys. Chem. C*, 2010, **114**, 251-255.
45. M.-Y. Cheng and B.-J. Hwang, *J. Power Sources*, 2010, **195**, 4977-4983.
46. X. Wang, X. Li, X. Sun, F. Li, Q. Liu, Q. Wang and D. He, *J. Mater. Chem.*, 2011, **21**, 3571-3573.
47. W. Zhang, M. Li, Q. Wang, G. Chen, M. Kong, Z. Yang and S. Mann, *Adv. Funct. Mater.*, 2011, **21**, 3516-3523.
48. L. Q. Lu and Y. Wang, *J. Mater. Chem.*, 2011, **21**, 17916-17921.
49. D. Bresser, E. Paillard, R. Kloepsch, S. Krueger, M. Fiedler, R. Schmitz, D. Baither, M. Winter and S. Passerini, *Adv. Energy Mater.*, 2013, **3**, 513-523.
50. S. Liu, J. Xie, C. Fang, G. Cao, T. Zhu and X. Zhao, *J. Mater. Chem.*, 2012, **22**, 19738-19743.
51. Y. Zhao, J. Li, Y. Ding and L. Guan, *J. Mater. Chem.*, 2011, **21**, 19101-19105.
52. G. Zhou, D.-W. Wang, P.-X. Hou, W. Li, N. Li, C. Liu, F. Li and H.-M. Cheng, *J. Mater. Chem.*, 2012, **22**, 17942-17947.
53. P. Poizot, S. Laruelle, S. Grugeon, L. Dupont and J. M. Tarascon, *Nature*, 2000, **407**, 496-499.
54. L. Su, Z. Zhou, X. Qin, Q. Tang, D. Wu and P. Shen, *Nano Energy*, 2012, **2**, 276-282.
55. W. A. Ang, N. Gupta, R. Prasanth and S. Madhavi, *ACS Appl. Mater. Interfaces*, 2012, **4**, 7011-7019.

This journal is © The Royal Society of Chemistry 2013

56. P. Liu, J. J. Vajo, J. S. Wang, W. Li and J. Liu, *J. Phys. Chem. C*, 2012, **116**, 6467-6473.
57. K. Xie, Z. Lu, H. Huang, W. Lu, Y. Lai, J. Li, L. Zhou and Y. Liu, *J. Mater. Chem.*, 2012, **22**, 5560-5567.
58. Q.-q. Xiong, J.-p. Tu, Y. Lu, J. Chen, Y.-x. Yu, X.-l. Wang and C.-d. Gu, *J. Mater. Chem.*, 2012, **22**, 18639-18646.
59. L. Su, Z. Zhou and P. Shen, *J. Phys. Chem. C*, 2012, **116**, 23974-23980.